Scripta Materialia 144 (2018) 48–51

Contents lists available at ScienceDirect

Scripta Materialia

journal homepage: www.elsevier.com/locate/scriptamat

Regular article

Elastocaloric effect in polycrystalline $Ni_{50}Ti_{45.3}V_{4.7}$ shape memory alloy

Yanghoo Kim [a], Min-Gu Jo [a], Ju-Won Park [a], Hyung-Ki Park [b], Heung Nam Han [a,*]

[a] Department of Materials Science and Engineering and Research Institute of Advanced Materials, Seoul National University, Seoul 08826, Republic of Korea
[b] Gangwon Regional Division, Korea Institute of Industrial Technology, Gangneung 25440, Republic of Korea

ARTICLE INFO

Article history:
Received 17 May 2017
Received in revised form 28 September 2017
Accepted 28 September 2017
Available online xxxx

Keywords:
Elastocaloric effect
Shape memory alloys
Martensitic phase transformation
Fatigue test

ABSTRACT

The elastocaloric effect and functional fatigue life of the polycrystalline $Ni_{50}Ti_{45.3}V_{4.7}$ shape memory alloy have been studied. Temperature changes on rapid loading and unloading of a mechanically trained specimen were directly measured at different compressive stress levels. It was found that the maximum elastocaloric strength was accomplished at the stress corresponding to the end point of a transformation plateau. In the fatigue test, no significant degradation occurred in the elastocaloric cooling ability after 5000 cyclic loadings. Compared to pure NiTi, the present alloy showed improved efficiency and endurance limit of the functional stability.

Caloric materials that undergo solid to solid phase transformation on the application of various driving fields have gathered much attention as alternatives for next-generation refrigeration systems owing to their merits such as eco-friendliness, fast response, and relatively simple setup compared to the conventional vapor compression cooling [1,2]. Among them, elastocaloric (EC) materials have assessed to be the most promising candidates in a 2014 report of US Department of Energy [3]. Essentially, the EC effect is quantified by the isothermal entropy change (ΔS_{iso}) or adiabatic temperature change (ΔT_{adi}); however, it needs to evaluate various parameters related to the efficiency, e.g. the EC cooling strength, coefficient of performance (COP), and operating temperature range, to select a suitable EC material. In addition, the fatigue properties during repetitive loadings are key factors that determine long-term use in a practical application.

Shape memory alloys (SMAs) exhibiting thermal response with first-order reversible martensitic transformation (MT) by external stress have been intensively investigated as suitable materials for the EC effect in recent years [4–8]. Although there are many classes of SMAs, depending on the chemical composition and functionality, NiTi has been a focus of interest in the research on SMAs. In view of the EC effect, NiTi shows a large temperature change (ΔT) but suffers from poor functional and structural stability [9,10]. Alloying of additional elements can help overcome this drawback. It was demonstrated that a NiTiCu film can withstand 10 million loading cycles [11] and shows a stable EC effect up to 1500 cycles without any evident degradation [12]. Additionally, a small functional fatigue effect was confirmed during thermomechanical training for NiTiCuV [13]. In a similar vein, the present work investigated the EC effect in V-added bulk NiTi using compression test which is more advantageous than tensile case in terms of mechanical fatigue due to crack propagation retardation [9,14]. The V concentration was selected so that the SMA shows superelasticity at room temperature (RT) and low transformation thermal hysteresis, which implies good reversibility of transformation with a compatible phase boundary between the parent austenite and martensite [15].

An ingot with a nominal composition of $Ni_{50}Ti_{45.3}V_{4.7}$ (at.%) was arc-melted in an argon atmosphere using high-purity elements (99.99 wt%). The total weight loss after seven re-melting processes was less than 0.1%. The ingot was homogenized in an evacuated quartz furnace at 1050 °C for 24 h followed by ice water quenching. Electron back scattered diffraction (EBSD) was utilized to characterize the initial microstructure of the parent austenite. The characteristic phase transformation temperatures, enthalpy change (ΔH), and specific heat capacity (C_p) were determined by differential scanning calorimetry (DSC) at a scanning rate of 10 °C min^{-1}. Before investigating the EC effect, a square prismatic specimen with dimensions of 5.0 mm × 5.0 mm × 9.0 mm was mechanically trained by 30 cyclic loadings with a compressive stress of 300 MPa at a strain rate of 0.001 s^{-1}. Subsequently, EC heating and cooling tests were performed at RT by applying and removing different stress levels in the range of 0–300 MPa at a strain rate of 0.025 s^{-1}. Each test was conducted separately. In the EC cooling test, the specimen was loaded isothermally at a strain rate of 0.0002 s^{-1} followed by holding for 5 s before unloading. The temperature of the central part of the specimen was directly monitored using an infrared thermal imaging camera. For the fatigue test, cyclic loadings were carried out with a compressive stress of 260 MPa for up to 5000 cycles with temperature monitoring at a strain rate of 0.03 s^{-1} followed by the same EC cooling test as performed on the trained specimen. (See

* Corresponding author.
E-mail address: hnhan@snu.ac.kr (H.N. Han).

https://doi.org/10.1016/j.scriptamat.2017.09.048
1359-6462/

real-time temperature changes of the specimen in Supplementary materials.)

Fig. 1(a) shows the characteristics of the thermally induced reversible MT obtained by DSC measurement. The martensitic start (M_s) and finish (M_f) and austenite start (A_s) and finish (A_f) temperatures are 4.6, −6.3, 7.5, and 14.7 °C, respectively. The values of ΔH in the MT and reverse MT were estimated as −9.04 and 9.40 J g^{-1}, respectively, and corresponding entropy changes (ΔS) were calculated as −31.98 and 33.26 J Kg^{-1} K^{-1} according to the following equation,

$$\Delta S = \Delta H / T_0 \tag{1}$$

where T_0 is the equilibrium temperature defined as $(A_f + M_s)/2$ [7]. The transformation thermal hysteresis, defined here as $(A_s + A_f - M_s - M_f)/2 = 12.0$ °C, was observed to be very small compared to that of NiTi or NiTiX [16]. As mentioned above, it implies that the MT of the present SMA is highly reversible and therefore stable fatigue properties are expected. Fig. 1(b) shows the inverse pole figure map of the austenite in the loading direction at RT for the specimen used in the EC test by EBSD. Large columnar grains perpendicular to the loading direction are observed with no specific texture development.

The compressive stress-strain (SS) curves obtained during mechanical training are shown in Fig. 2. In the early stage of the training, residual strain is evident but the final SS curve shows perfect superelasticity with complete strain recovery. The blue solid line represents the corrected SS curve of the final cycle considering the dimensional change originated from the plastic deformation in the grains with poor orientation for transformation [17]. It means that the micro-scale strain evolution and corresponding spatial distribution of thermal response during loading cycle are inhomogeneous. This heterogeneity of the phase transformation, occurring even in single crystals depending on the alloy composition, lowers the efficiency of the EC effect [14]. Therefore, proper texture development is desired for better performance of the EC effect in polycrystalline SMAs. Comparing the first and final cycles clearly demonstrates that several aspects of the superelastic behavior change gradually. The critical stress for the stress-induced MT (σ_s) decreases from 134 to 81 MPa, which can be attributed to the internal stress of dislocations generated during the training cycles [18]. The slopes of the transformation plateau in loading and unloading become steeper so that the trained SS curve is narrow with a small transformation stress hysteresis.

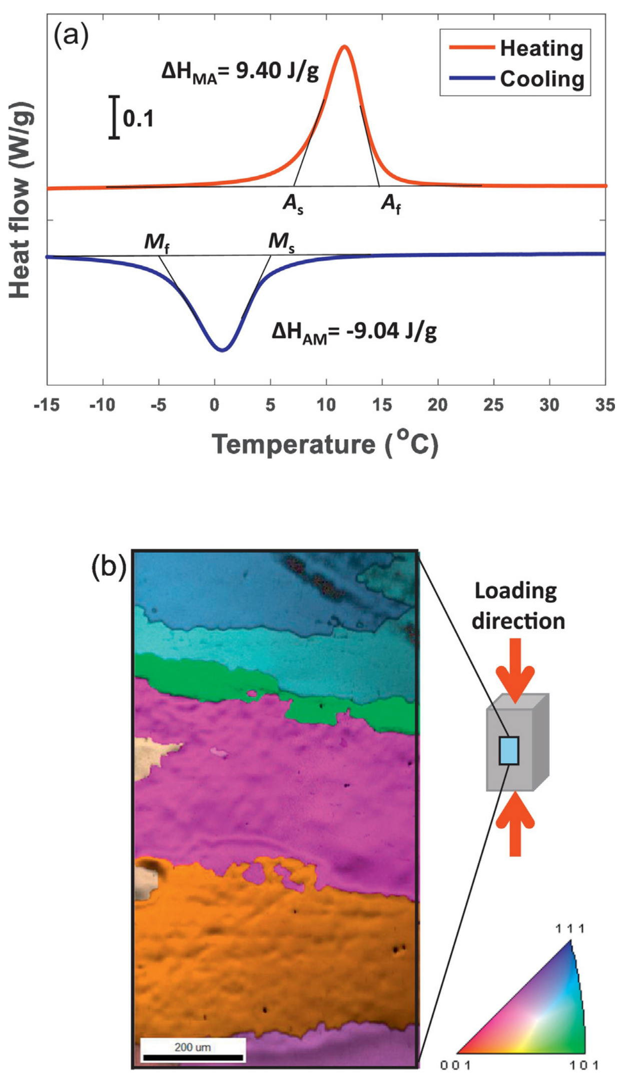

Fig. 1. (a) DSC curve with a scanning rate of 10 °C min^{-1}. The subscripts M and A of ΔH refer to martensite and austenite, respectively. (b) Inverse pole figure map of the austenite in the loading direction at RT for the specimen used in the EC test by EBSD.

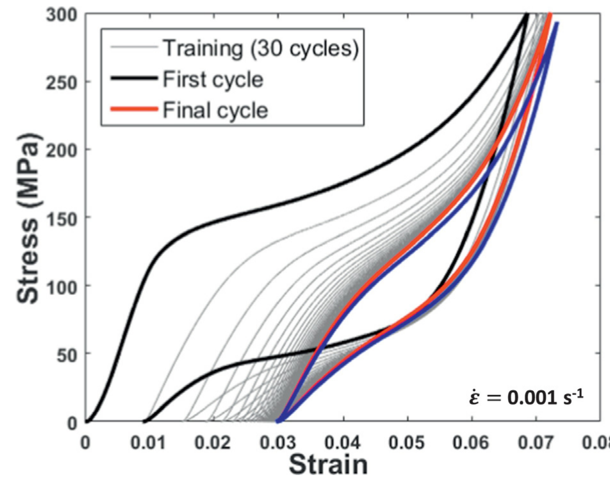

Fig. 2. Compressive SS curves during the mechanical training of 30 cyclic loadings at RT. The blue solid line represents the corrected SS curve of the final cycle considering the dimensional change during the training. (For interpretation of the references to colour in this figure legend, the reader is referred to the web version of this article.)

Fig. 3(a) shows the ΔT against the different stress levels, divided into three regions—R1, R2, and R3—based on the critical stresses (σ_s and σ_f) in the loading part of the final SS curve in Fig. 2. Interestingly, a finite ΔT is observed for R1, which can be regarded as the pure elastic part of the austenite in macroscopic scope, suggesting that a small fraction of the austenite was transformed to martensite. In R2, corresponding to the transformation plateau, ΔT increases linearly with the stress. In R3, which is the elastic part of the transformed martensite in macroscopic scope, the stress-induced MT is almost complete. However, the small increase in the ΔT can be explained by the transformation of the remaining austenite. Using C_p (=0.51 J g^{-1} K^{-1}), the theoretical ΔT_{adi} was estimated as 18.6 °C for the EC heating and −19.4 °C for the EC cooling according to the following equation,

$$\Delta T_{adi} = -T \cdot \Delta S / C_p \tag{2}$$

where T is the ambient temperature. When comparing ΔT_{adi} to the measured ΔT for the largest stress level of 290 MPa, the differences seems somewhat large, which can be explained by the fact that the strain rate used for the EC test was not sufficient for the ideal adiabatic process and the transformation was not complete by 290 MPa and further loading was necessary to complete the transformation. Fig. 3(b) shows the corresponding strength of EC effect, $|\Delta T/\Delta\sigma|$, at the stress levels in Fig. 3(a). In both cases, the strengths of EC effect accomplished a maximum value slightly larger than 50 °C GPa^{-1} at the stress of about